NDT net e-Journal of Nondestructive Testing - ISSN 1435-4934 - www.ndt.net

14th Conference on Industrial Computed Tomography, Antwerp, Belgium (iCT 2025), www.ICT2025.org

Application Assessment of OS-SART Reconstruction Algorithm with Limited Number of Projections in XCT Geometric Measurement

Kaojie Yue[1], Huan Shao[1], Stefano Petrò[1], Giovanni Moroni[1]

[1] Department of Mechanical Egineering, Politecnico di Milano, Via La Masa 1, Milano 20156, Italy, e-mail: kaojie.yue@polimi.it

Abstract

In industrial X-ray Computed Tomography (XCT), two primary kinds of reconstruction algorithms are utilized: the Feldkamp-Davis-Kress (FDK) algorithm and the algebraic reconstruction technique (ART) algorithms. While the FDK algorithm is predominantly employed in industrial XCT due to its competitive efficiency, it necessitates a large number of projections (*Np*) to yield good 3D images. Conversely, although ART algorithms require relatively longer computational times, their mechanism enables volume reconstruction with a smaller number of projections, thereby offering a potential advantage in scenarios with limited *Np*. To rigorously investigate the potential of ART algorithms under conditions of limited *Np*, this study focuses on the ordered subsets simultaneously algebraic reconstruction technique (OS-SART) algorithm, a classic ART algorithm. A series of experiments is conducted, targeting three key algorithmic parameters. These experiments are based on a stepped cylinder part across varying *Np* levels, with the error between the values of XCT measurement and coordinate measurement machine as the evaluation metric. Eventually, the impacts of these parameters are evaluated based on the experimental results.

Keywords: X-ray computed tomography, Dimensional measurement, Reconstruction algorithm, OS-SART

1 Introduction

With the development of Industrial X-ray Computed Tomography (XCT) and the increasing demand for high-quality parts, the application of XCT in dimensional measurement is expanding. One of the main challenges associated with this technique is the lengthy acquisition time, primarily attributed to the number of projections (*Np*) and the exposure time [1]. In a traditional full scan, where the detector size is approximately 2000×2000, thousands of projection images are necessary to obtain reliable results [2]. This requirement can result in acquisition times ranging from tens to hundreds of minutes for a single scan. In recent years, many studies have focused on reducing acquisition times, with decreasing *Np* identified as a direct solution [1].

However, *Np*, which determines the data amount for the reconstruction process, generally influences the measurement results. Currently, the mostly used reconstruction algorithm in industrial XCT is Feldkamp-Davis-Kress (FDK) algorithm, which specifies a minimum *Np* based on the Nyquist-Shannon sampling theorem [3]. Aiming to reduce Np and improve the measurement efficiency, Villarraga-Gómez et al. [4] studied the effects of *Np* on dimensional measurements using the FDK reconstruction algorithm. It turned out that for size dimensions (diameter, length, and hole distance), *Np* could be reduced by around 70% compared to the *Np* required for a full scan. While for form deviations (cylindricity and flatness), *Np* should not be reduced.

Besides FDK, the typical analytical algorithm, algebraic reconstruction technique (ART) algorithms have also been applied in medical research. For ART algorithms, the reconstruction problem is approached as solving a system of equations, with each equation representing the attenuation process along a discrete X-ray path. More details can be found in reference [5]. The three fundamental ART algorithms are Algebraic Reconstruction Technique, Simultaneous Algebraic Reconstruction Technique (SART), and Simultaneous Iterative Reconstruction Technique (SIRT). These algorithms solve the reconstruction problem by iteratively updating the unknowns to minimize the difference between real projections and the projections generated from the reconstructed volume [6]. Among these algorithms, SIRT updates the unknowns all-at-once, presenting significant potential for parallel computation. In contrast, Algebraic Reconstruction Technique exhibits limited potential for parallelization since it updates the unknowns ray-by-ray. SART offers a balanced approach, updating the unknowns image-by-image. To offer flexible control over computational accuracy and speed, Ordered-subset Simultaneous Algebraic Reconstruction (OS-SART) has been proposed, in which subsets are defined by a specified number of equations or projections, allowing the unknowns to be updated for each subset [7]. Generally, each subset contains multiple projections, facilitating better parallel computation compared to SART.

In recent years, ART algorithms have been studied and evaluated for XCT dimensional measurements, particularly in scenarios with limited *Np*. Jones et al. [8] tested the performance of several ART algorithms in the measurement of wall thickness, including algebraic reconstruction technique, SIRT, algebraic reconstruction technique with total variation (TV) regularization, and gradient decent with TV regularization. They found that ART algorithms perform well even with fewer *Np*. Sun et al. [9] evaluated two ART algorithms, OS-SART and Ordered-subset Adaptive Steepest Descent Projection onto Convex Set (OS-ASD-POCS), for measurements on diameter and edge distance with only 60 simulated projection images (less than 2% of a full scan). Their results indicated that OS-ASD-POCS including TV regularization can handle an extremely limited *Np*, and the measurement results are close to the nominal values. In contrast, the FDK algorithm does not provide reliable measurement

https://doi.org/10.58286/30737

results with such a limited *Np*. These studies suggest that ART algorithms possess strong potential for tasks involving limited *Np*.

In the application of ART algorithms, certain parameters can significantly influence performance. For instance, in the OS-SART algorithm, key parameters include subset selection strategy, initial values, and number of iterations, etc. [7]. Usually, the settings for these parameters are determined based on experience or software recommendations. However, their impact on measurement results remains unclear, particularly in scenarios with limited *Np*. This indicates that parameter settings optimized for full scans may not be applicable, which could undermine the reliability of the measurement results. Consequently, it is crucial to explore how these parameters affect measurement outcomes in scenarios with limited *Np*. In this paper, we inspected the influence of subset selection strategy, initial value and number of iterations in OS-SART algorithm with varying *Np*. One size dimension (diameter) and two form deviations (cylindricity and flatness) on a multi-cylinder part were measured. Analysis of variance (ANOVA) was conducted to assess the influence of the abovementioned factors.

2 Method

2.1 Data collection

A stepped cylinder part was scanned using a Phoenix V|tome|x M300 XCT system (Figure 1) equipped with a 300 kV microfocus X-ray tube and a Dynamic 41|100 detector with 2016×2016 pixels, each with a physical size of 0.2 mm × 0.2 mm. The part was positioned on a foam support, with its axis aligned at a 45° angle relative to the rotation axis of the XCT machine. The scan parameters outlined in Table 1 were chosen to ensure reliable results. The scan was repeated twice with repositioning. A total of 2016 ($N_{p,full}$) projections were collected per scan, referred to as a "full scan". Subsequently, datasets with limited *Np* were extracted uniformly from the full scans. Before XCT scans, the part was calibrated using a Zeiss Prismo VAST HTG coordinate measuring machine (CMM). Calibrated values are shown in Table 2.

Table 1: Scan parameters

Scan parameters	Setting points
Voxel size /µm	25.055
X-ray tube voltage /kV	250
X-ray tube current /µA	110
Exposure time / ms	100
Scan mode	Start/stop
Average	3
Number of projections	2016
Filter material	Sn
Filter thickness /mm	1.0
Binning	1×1
Image resolution	2016×2016

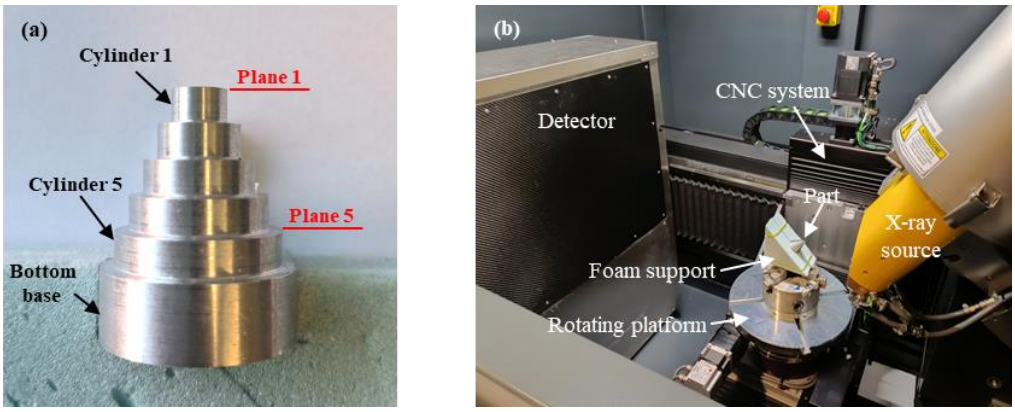

Figure 1: Experiment configurations. (a) part geometry and (b) the X-ray computed tomography system.

Table 2 Measurands and calibrated values. *U* is the expanded uncertainty with the coverage factor *k* equal to 2.

Type	Measurand	Name	Nominal value /mm	Calibrated value /mm	*U* /µm
Size dimensions	Diameter of cylinder 1	D1	8	7.996	0.5
	Diameter of cylinder 2	D2	12	11.994	0.2
	Diameter of cylinder 3	D3	16	15.992	0.3
	Diameter of cylinder 4	D4	20	19.988	0.2
	Diameter of cylinder 5	D5	24	23.984	0.1
Form deviations	Cylindricity of cylinder 1	Cy1	N/A	0.005	1.7
	Cylindricity of cylinder 2	Cy2	N/A	0.005	0.7
	Cylindricity of cylinder 3	Cy3	N/A	0.005	1.0
	Cylindricity of cylinder 4	Cy4	N/A	0.005	0.5
	Cylindricity of cylinder 5	Cy5	N/A	0.004	0.5
	Flatness of plane 1	F1	N/A	0.006	1.5
	Flatness of plane 2	F2	N/A	0.005	0.9
	Flatness of plane 3	F3	N/A	0.007	1.4
	Flatness of plane 4	F4	N/A	0.004	0.7
	Flatness of plane 5	F5	N/A	0.004	0.8

2.2 Data processing

Between acquisition and reconstruction, a few processes are conducted on the raw projections. First, dark field correction and flat field correction were applied automatically by acquisition software. Subsequently, a 3×3 median filtering was applied to all images to suppress random noise generated by the XCT system [10]. In order to eliminate beam-hardening effects, beam-hardening correction (BHC) was determined based on the Equation (2) with presets provided by CT Pro 3D XT 2.2 SP10 software [11]:

$$Y = a(b + cX + dX^2 + eX^3 + fX^4) \quad (2)$$

where X presents the raw gray values in raw images, and Y denotes the corrected gray values corresponding to X. The preset coefficients selected in this work are as follows: $a = 1, b = 0, c = 1, d = 0, e = 0, f = 0$. Then, all projections containing the X-ray intensity were converted to the line integral value, based on the Beer-Lambert law. In addition, the rotation axis offset was directly obtained from the XCT system, while the horizontal detector offset was calculated in the reconstruction module of VGStudio Max [12]. These two offset values were applied to the reconstruction process to correct the geometric misalignments. OS-SART algorithm was used for the reconstruction offered by TIGRE [13], a graphic process unit (GPU) based reconstruction toolkit and was executed in Matlab 2022b. The main parameters of the algorithm include subset selection strategy, subset number/size, initial value, and number of iterations. The relaxation factor influences the convergence of the computation, and the optimum may be relevant to the specific task. The default value of 1.0 was selected in this work. The input projections were divided into several subsets with a certain size. For the full scan with 2016 projections, subset number and subset size were set as 126 and 16 respectively to achieve acceptable results and computation time. With varying *Np*, the subset selection strategy can be constant subset number (*Cn*) or constant subset size (*Cs*). Since the ending policy in OS-SART algorithm is the pre-defined number of iterations, three levels of number of iterations were set as 5, 10, and 15. Two levels of initial values were $\boldsymbol{x_0}$, and $\boldsymbol{x_{FDK}}$, in which $\boldsymbol{x_0}$ represents that all unknowns are zero, while $\boldsymbol{x_{FDK}}$ means that the initial value is calculated by FDK algorithm using the input dataset with the given *Np*. All the combinations were performed with varying *Np* level equal to $k{\cdot}N_{p,full}$, where k is a coefficient with levels of 1, 1/4, and 1/16. The factors and levels are listed in Table 3.

Table 3: Factors and levels in experiments.

Factors	Levels
K	1, 1/4, 1/16
Subset selection strategy	*Cn*, *Cs*
Initial value	$\boldsymbol{x_0}$, $\boldsymbol{x_{FDK}}$
Number of iterations	5, 10, 15

Surface determination was performed in VGStudio Max using the "advanced (classic)" method with the initial contour determined by ISO50 method, and the iterative surface determination option was used [12]. Feature fitting and measurement

were also conducted in VGStudio Max, employing "Gaussian (least squares)" method for diameters and "Chebyshev (minimum zone)" method for cylindricity and flatness deviations. ANOVA was conducted to analyze the measurement result, with the error between XCT measurement results and calibrated sizes/deviations used as the response variable. Both normality and equal variance tests on the fit residuals were successfully passed.

3 Results

After reconstruction and surface determination processes, the surfaces of all treatments in the design of experiment are obtained. When *Np* is equal to 1/16 $N_{p,full}$, the obtained surfaces using *Cs* strategy reveal significant errors compared to those obtained with $N_{p,full}$, as shown in Figure 2. With the initial value of $\boldsymbol{x_0}$, the surface appears smooth but exhibits considerable shape error. While with $\boldsymbol{x_{FDK}}$ as the initial value, the surface is quite rough. This may be due to the update process in the reconstruction. In OS-SART, all unknowns are updated after the computation for each subset. Thus, in the *Cn* strategy, the number of updates remains constant and same as the reconstruction with $N_{p,full}$. However, in the *Cs* strategy, as *Np* decreases, the number of subsets is reduced, leading to a decrease in the number of updates for the unknowns. Based on studies of ART algorithms, this reduction in number of updates negatively impacts the accuracy of the computations [14]. Therefore, the analysis was separated in the following sections. The analysis for subset selection strategy focuses on the treatments with 1/4 $N_{p,full}$, while the analysis for initial value and number of iterations focuses on the treatments containing *Cn* strategy.

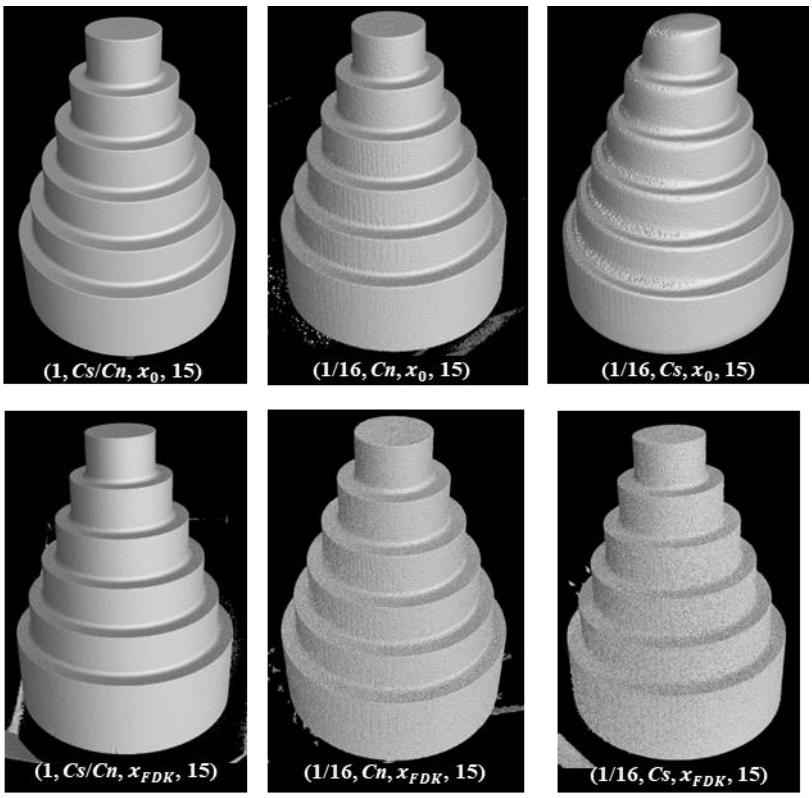

Figure 2: Volumes from reconstructions with different parameter treatments denoted at the bottom. Treatments are denoted by (*k, subset selection strategy, initial value, number of iterations*).

In the first analysis, ANOVA indicates that the subset selection strategy significantly influences all three measurands. To further clarify the impact of the subset selection strategy, Tukey comparison results and interaction plots are presented in Table 4 and Figure 3, respectively. For diameter measurements, most treatments fall into the same group (Group B), except for (1/4, *Cn*, $\boldsymbol{x_0}$, 5) and (1/4, *Cs*, $\boldsymbol{x_0}$, 5). This indicates that when the number of iterations is small, the subset selection strategy exhibits significant influences. However, when the number of iterations is greater than 5, no significant differences are observed, which is consistent with Figure 3. Thus, using more than 5 iterations, or using $\boldsymbol{x_{FDK}}$ as the initial value yields the better results.

In cylindricity measurements, significant influence from the subset selection strategy is generally absent when the initial value and number of iterations are the same, except for the treatments of (1/4, *Cn*, $\boldsymbol{x_0}$, 5) and (1/4, *Cs*, $\boldsymbol{x_0}$, 5). Using $\boldsymbol{x_0}$ as the initial value along with at least 10 iterations can achieve the better results. For flatness measurements, the *Cs* strategy with 15 iterations and the *Cn* strategy with at least 10 iterations achieve the better results. Therefore, using the *Cn* strategy can reduce the number of iterations while still delivering optimal performance.

The ANOVA for initial value and number of iterations was performed with the fixed subset selection strategy of *Cn*. The results indicate that both factors, along with *Np*, significantly influence the measurement results. Main effect plots are presented in Figure 4. For diameter measurements, the effects of *Np* and initial value are obvious. While for the measurements on cylindricity

and flatness deviations, all three factors show apparent effects. The interaction plots in Figure 5 suggest that both initial value and number of iterations have strong interaction with *Np*, with this interaction being particularly obvious in diameter measurements.

Table 4: Tukey comparison results. Treatments are denoted as (*Np*, *subset selection strategy*, *initial value*, *number of iterations*). Treatments that do not share a letter are significantly different. The means are expressed in micrometers.

Error of diameter			**Error of cylindricity deviation**			**Error of flatness deviation**		
Treatments	**Means**	**Grouping**	**Treatments**	**Means**	**Grouping**	**Treatments**	**Means**	**Grouping**
1/4, *Cn*, $\boldsymbol{x_0}$, 5	34.1	A	1/4, *Cs*, $\boldsymbol{x_{FDK}}$, 5	80.8	A	1/4, *Cs*, $\boldsymbol{x_0}$, 5	168.0	A
1/4, *Cn*, $\boldsymbol{x_0}$, 10	-0.9	B	1/4, *Cn*, $\boldsymbol{x_0}$, 5	76.2	A B	1/4, *Cs*, $\boldsymbol{x_{FDK}}$, 5	62.0	B
1/4, *Cs*, $\boldsymbol{x_{FDK}}$, 5	-1.1	B	1/4, *Cn*, $\boldsymbol{x_{FDK}}$, 5	73.8	A B C	1/4, *Cs*, $\boldsymbol{x_{FDK}}$, 10	60.7	B
1/4, *Cs*, $\boldsymbol{x_{FDK}}$, 10	-1.2	B	1/4, *Cn*, $\boldsymbol{x_{FDK}}$, 10	60.9	B C D	1/4, *Cs*, $\boldsymbol{x_{FDK}}$, 15	59.1	B C
1/4, *Cs*, $\boldsymbol{x_{FDK}}$, 15	-1.3	B	1/4, *Cs*, $\boldsymbol{x_{FDK}}$, 10	60.5	B C D	1/4, *Cn*, $\boldsymbol{x_{FDK}}$, 5	57.7	B C
1/4, *Cn*, $\boldsymbol{x_{FDK}}$, 5	-1.5	B	1/4, *Cs*, $\boldsymbol{x_{FDK}}$, 15	57.8	C D	1/4, *Cn*, $\boldsymbol{x_{FDK}}$, 10	56.2	B C
1/4, *Cs*, $\boldsymbol{x_0}$, 15	-1.5	B C	1/4, *Cn*, $\boldsymbol{x_{FDK}}$, 15	56.4	D	1/4, *Cn*, $\boldsymbol{x_0}$, 5	54.0	C
1/4, *Cn*, $\boldsymbol{x_0}$, 15	-1.5	B C	1/4, *Cs*, $\boldsymbol{x_0}$, 5	51.0	D	1/4, *Cn*, $\boldsymbol{x_{FDK}}$, 15	53.5	C
1/4, *Cs*, $\boldsymbol{x_0}$, 10	-1.9	B C	1/4, *Cn*, $\boldsymbol{x_0}$, 15	32.1	E	1/4, *Cs*, $\boldsymbol{x_0}$, 10	41.5	D
1/4, *Cn*, $\boldsymbol{x_{FDK}}$, 10	-2.0	B C	1/4, *Cn*, $\boldsymbol{x_0}$, 10	29.5	E	1/4, *Cs*, $\boldsymbol{x_0}$, 15	25.0	E
1/4, *Cn*, $\boldsymbol{x_{FDK}}$, 15	-2.3	B C	1/4, *Cs*, $\boldsymbol{x_0}$, 10	28.8	E	1/4, *Cn*, $\boldsymbol{x_0}$, 15	23.5	E
1/4, *Cs*, $\boldsymbol{x_0}$, 5	-3.8	C	1/4, *Cs*, $\boldsymbol{x_0}$, 15	25.9	E	1/4, *Cn*, $\boldsymbol{x_0}$, 10	22.1	E

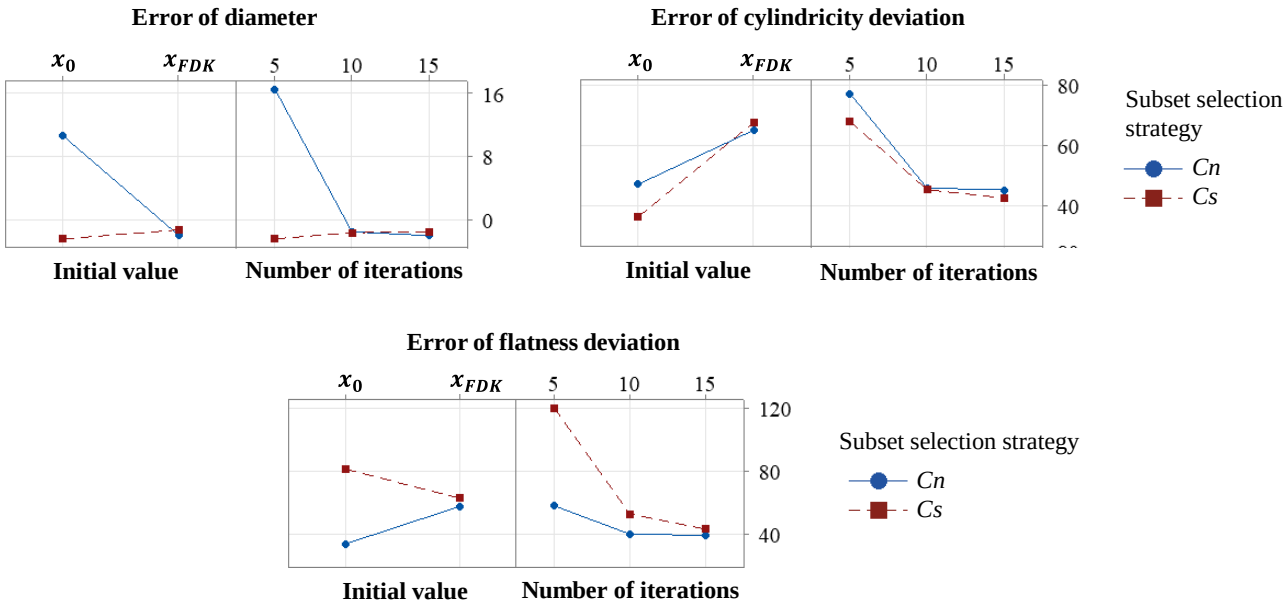

Figure 3: Interaction plots among subset selection strategy, initial value and number of iterations. The values along vertical axes represent the mean error between XCT and CMM results.

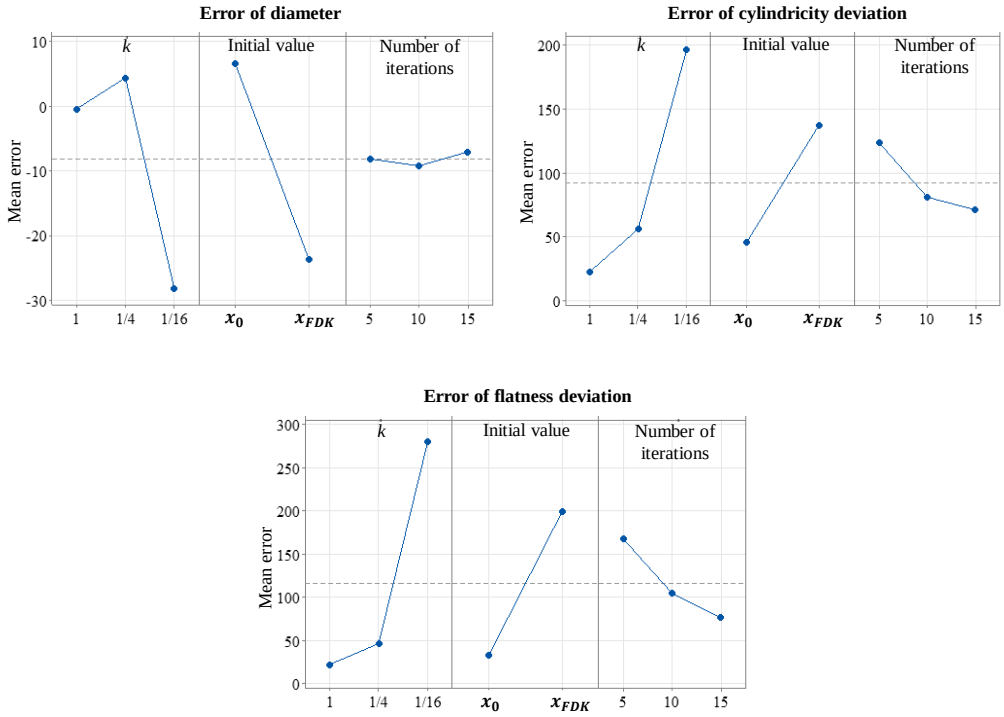

Figure 4: Main effect plots. The values along vertical axes represent the mean error between XCT and CMM results.

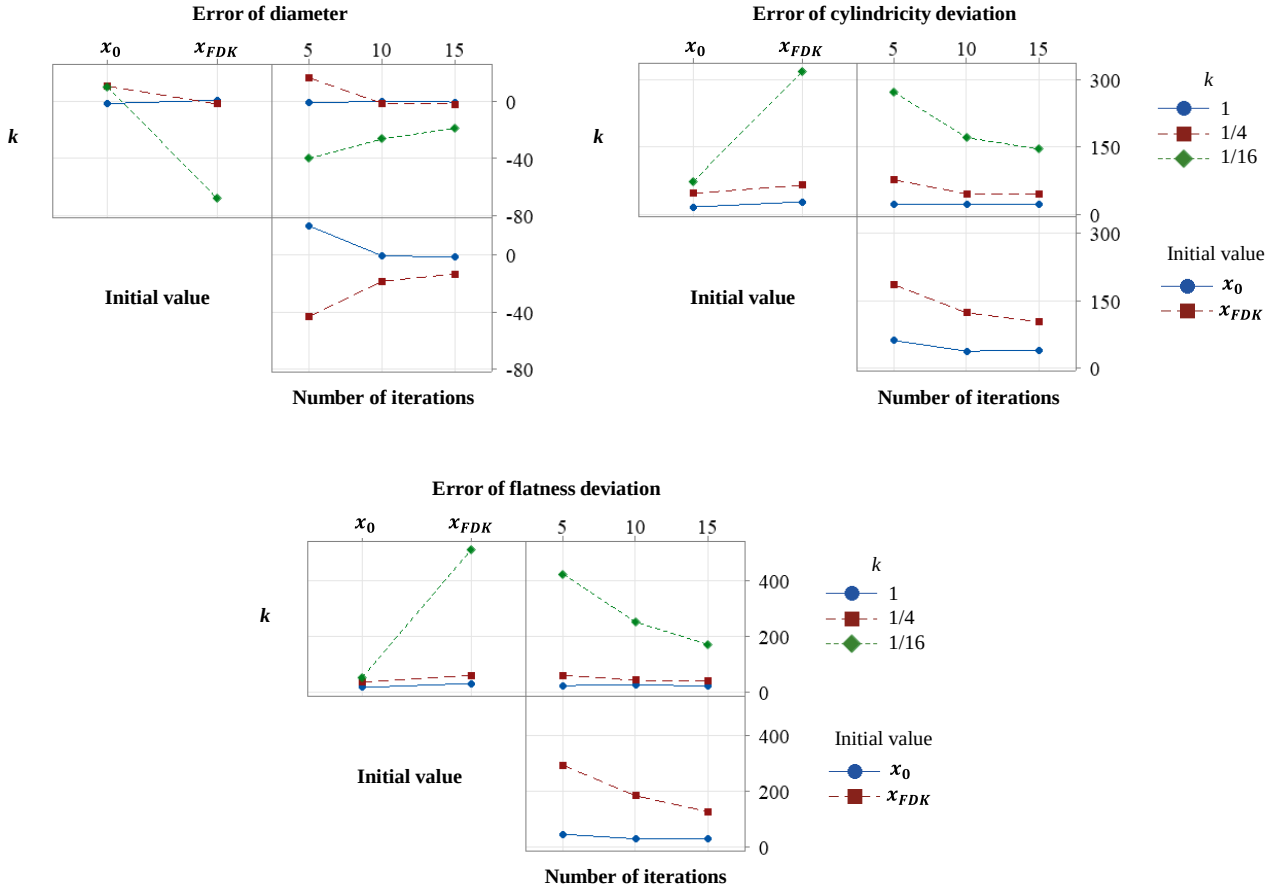

Figure 5: Interaction plots among k, initial value, and number of iterations. The values along vertical axes represent the mean error between XCT and CMM results.

Tukey comparison results are presented in Table 5. For diameter measurements, when *Np* is equal to $N_{p,full}$, the treatments with any initial value do not show significant differences compared to (1, $\boldsymbol{x_0}$, 15) or (1, $\boldsymbol{x_{FDK}}$, 15). However, when *Np* is equal to 1/4 $N_{p,full}$, the treatment (1/4, $\boldsymbol{x_0}$, 5) is significantly different from all treatments with $N_{p,full}$, while the treatment (1/4, $\boldsymbol{x_{FDK}}$, 5) is not. This suggests that using $\boldsymbol{x_{FDK}}$ as the initial value can improve the results. When *Np* is equal to 1/16 $N_{p,full}$, all treatment with $\boldsymbol{x_{FDK}}$ as the initial value are significantly different from those with $N_{p,full}$. However, the treatment (1/16, $\boldsymbol{x_0}$,10) and (1/16, $\boldsymbol{x_0}$, 15) do not show significant differences. This indicates that with an insufficient *Np*, using $\boldsymbol{x_{FDK}}$ as the initial value can lead to worse results. This may be attributed to artefacts arising from the use of FDK algorithm with very few projections [15]. In cylindricity measurements, using $\boldsymbol{x_{FDK}}$ as the initial value does not improve the results. In fact, for any treatment with the initial value of $\boldsymbol{x_0}$, switching to $\boldsymbol{x_{FDK}}$ significantly worsens the result. A similar trend can be observed in flatness measurement results. For number of iterations, Tukey comparison results indicate that when *Np* is equal to $N_{p,full}$, the number of iterations does not significantly influence the results. This can also be observed in the interaction plots, where the results with $N_{p,full}$ (represented by blue lines) remain consistent. However, with 1/4 $N_{p,full}$, the treatment (1/4, $\boldsymbol{x_0}$, 5) is in a different group from the treatment (1/4, $\boldsymbol{x_0}$, 10) and (1/4, $\boldsymbol{x_0}$, 15) across all measurands. When *Np* is further reduced to 1/16 $N_{p,full}$, the number of iterations has a more significant influence on the results.

Table 5: Tukey comparison results. Treatments are denoted as (*Np*, *subset selection strategy*, *initial value*, *number of iterations*). Treatments that do not share a letter are significantly different. The means are expressed in micrometers.

Error of diameter			**Error of cylindricity deviation**			**Error of flatness deviation**		
Treatments	**Means**	**Grouping**	**Treatments**	**Means**	**Grouping**	**Treatments**	**Means**	**Grouping**
1/4, $\boldsymbol{x_0}$, 5	34.6	A	1/16, $\boldsymbol{x_{FDK}}$, 5	437.2	A	1/16, $\boldsymbol{x_{FDK}}$, 5	655.3	A
1/16, $\boldsymbol{x_0}$, 5	30.4	B	1/16, $\boldsymbol{x_{FDK}}$, 10	273.7	B	1/16, $\boldsymbol{x_{FDK}}$, 10	384.0	A B
1, $\boldsymbol{x_{FDK}}$, 5	1.8	C	1/16, $\boldsymbol{x_{FDK}}$, 15	220.5	B	1/16, $\boldsymbol{x_{FDK}}$, 15	262.6	B
1/16, $\boldsymbol{x_0}$, 10	1.3	C D	1/16, $\boldsymbol{x_0}$, 5	87.6	C	1/4, $\boldsymbol{x_{FDK}}$, 5	55.1	C
1, $\boldsymbol{x_{FDK}}$, 10	1.2	C D	1/4, $\boldsymbol{x_0}$, 5	76.2	C D	1/16, $\boldsymbol{x_0}$, 5	54.6	C
1, $\boldsymbol{x_{FDK}}$, 15	0.7	C D	1/4, $\boldsymbol{x_{FDK}}$, 5	73.8	C D	1/4, $\boldsymbol{x_{FDK}}$, 10	53.7	C D
1/16, $\boldsymbol{x_0}$, 15	-0.2	C D	1/16, $\boldsymbol{x_0}$, 15	66.2	D E	1/4, $\boldsymbol{x_{FDK}}$, 15	51.3	C D
1/4, $\boldsymbol{x_0}$, 10	-0.9	C D	1/16, $\boldsymbol{x_0}$, 10	62.1	D E	1/4, $\boldsymbol{x_0}$, 5	50.6	C D
1, $\boldsymbol{x_0}$, 10	-1.1	C D	1/4, $\boldsymbol{x_{FDK}}$, 10	60.9	D E	1/16, $\boldsymbol{x_0}$, 15	44.5	C D E
1/4, $\boldsymbol{x_{FDK}}$, 5	-1.4	C D	1/4, $\boldsymbol{x_{FDK}}$, 15	56.4	E	1/16, $\boldsymbol{x_0}$, 10	43.3	C D E
1/4, $\boldsymbol{x_0}$, 15	-1.5	C D	1/4, $\boldsymbol{x_0}$, 15	32.1	F	1 $\boldsymbol{x_{FDK}}$, 10	30.2	D E F
1, $\boldsymbol{x_0}$, 15	-1.6	C D	1/4, $\boldsymbol{x_0}$, 10	29.5	F	1, $\boldsymbol{x_{FDK}}$, 5	26.4	E F
1, $\boldsymbol{x_0}$, 5	-1.9	D	1, $\boldsymbol{x_{FDK}}$, 15	28.0	F	1, $\boldsymbol{x_{FDK}}$, 15	25.5	E F
1/4, $\boldsymbol{x_{FDK}}$, 10	-1.9	D	1, $\boldsymbol{x_{FDK}}$, 10	27.7	F	1/4, $\boldsymbol{x_0}$, 15	22.9	F G
1/4, $\boldsymbol{x_{FDK}}$, 15	-2.2	D	1, $\boldsymbol{x_{FDK}}$, 5	27.6	F	1/4, $\boldsymbol{x_0}$, 10	21.5	F G H
1/16, $\boldsymbol{x_{FDK}}$, 15	-37.1	E	1, $\boldsymbol{x_0}$, 10	18.5	G	1, $\boldsymbol{x_0}$, 5	14.0	G H
1/16, $\boldsymbol{x_{FDK}}$, 10	-52.1	F	1, $\boldsymbol{x_0}$, 15	16.9	G	1, $\boldsymbol{x_0}$, 10	13.7	H
1/16, $\boldsymbol{x_{FDK}}$, 5	-91.3	G	1, $\boldsymbol{x_0}$, 5	14.7	G	1, $\boldsymbol{x_0}$, 15	13.4	H

4 Discussion and conclusion

This paper investigates the effects of three main parameters in OS-SART algorithm, subset selection strategy, initial value, and number of iterations, on XCT dimensional measurements with varying *Np*. Results indicate that when using number of iterations as the ending policy, the subset selection strategy *Cn* delivers consistent performance and reliable results at both 1/4 $N_{p,full}$ and 1/16 $N_{p,full}$. In contrast, *Cs* performs well at 1/4 $N_{p,full}$ but fails to achieve effective reconstructions at 1/16 $N_{p,full}$. Therefore, from an industrial application perspective, *Cn* seems to be the more suitable subset selection strategy when using number of iterations as the ending policy. Additionally, one potential future research may aim to refine or design an ending policy for the OS-SART algorithm under limited *Np*, in order to further enhance computational efficiency and reconstruction quality.

The analysis of initial value and number of iterations suggests that when *Np* is close to $N_{p,full}$, these parameters have minimal impact on measurement results. With limited *Np*, although using $\boldsymbol{x_{FDK}}$ as the initial value can improve results in diameter measurements (see treatment (1/4, $\boldsymbol{x_0}$, 5)), it typically contributes to better measurement results of cylindricity and flatness deviations. When *Np* is further reduced, such as to 1/16 $N_{p,full}$, using $\boldsymbol{x_{FDK}}$ as the initial value would cause worse results. In contrast, starting with $\boldsymbol{x_0}$ and using no fewer than 10 iterations can provide the better results.

Acknowledgements

We gratefully acknowledge MICS (Made in Italy – Circular and Sustainable) Extended Partnership and received funding from the European Union Next-GenerationEU (Piano Nazionale di Ripresa e Resilienza (PNRR) – Missione 4 Componente 2, Investimento 1.3 – D.D. 1551.11-10-2022, PE00000004). We also express great appreciation for the support of the China Scholarship Council.

References

[1] E.A. Zwanenburg, M.A. Williams, J.M. Warnett, Review of high-speed imaging with lab-based x-ray computed tomography, Meas. Sci. Technol. 33 (2021) 012003.
[2] L. Körner, S. Lawes, D. Bate, L. Newton, N. Senin, R. Leach, Increasing throughput in x-ray computed tomography measurement of surface topography using sinogram interpolation, Meas. Sci. Technol. 30 (2019) 125002.
[3] J. Hsieh, Computed tomography: principles, design, artifacts, and recent advances, second ed., SPIE press, Washington, 2003.
[4] H. Villarraga-Gómez, S.T. Smith, Effect of the number of projections on dimensional measurements with X-ray computed tomography, Precis. Eng. 66 (2020) 445–456.
[5] S. Carmignato, W. Dewulf, R. Leach, Industrial X-ray computed tomography, first ed., Springer, 2018.
[6] A.H. Andersen, A.C. Kak, Simultaneous Algebraic Reconstruction Technique (SART): A Superior Implementation of the Art Algorithm, Ultrason. Imaging 6 (1984) 81–94.
[7] G. Wang, M. Jiang, Ordered-subset simultaneous algebraic reconstruction techniques (OS-SART), J. X-Ray Sci. Technol. 12 (2004) 169–177.
[8] G.A. Jones, P. Huthwaite, Limited view X-ray tomography for dimensional measurements, NDT E Int. 93 (2018) 98–109.
[9] W. Sun, S. Chretien, A. Biguri, M. Soleimani, T. Blumensath, J. Talbott, The realisation of fast X-ray computed tomography using a limited number of projection images for dimensional metrology, NDT E Int. 137 (2023) 102852.
[10] F. Zanini, L. Pagani, E. Savio, S. Carmignato, Characterisation of additively manufactured metal surfaces by means of X-ray computed tomography and generalised surface texture parameters, CIRP Ann. 68 (2019) 515–518.
[11] W. Dewulf, Y. Tan, K. Kiekens, Sense and non-sense of beam hardening correction in CT metrology, CIRP Ann. 61 (2012) 495–498.
[12] VGSTUDIO MAX, Industrial CT Software | Volume Graphics (n.d.). https://www.volumegraphics.com/en/products/vgsm.html (accessed September 16, 2024).
[13] A. Biguri, M. Dosanjh, S. Hancock, M. Soleimani, TIGRE: a MATLAB-GPU toolbox for CBCT image reconstruction, Biomed. Phys. Eng. Express 2 (2016) 055010.
[14] Y. Censor, D. Gordon, R. Gordon, BICAV: a block-iterative parallel algorithm for sparse systems with pixel-related weighting, IEEE Trans. Med. Imaging 20 (2001) 1050–1060.
[15] C. Rossides, H. Towsyfyan, A. Biguri, H. Deyhle, R. Lindroos, M. Mavrogordato, R. Boardman, W. Sun, T. Blumensath, Effects of fast x-ray cone-beam tomographic measurement on dimensional metrology, Metrologia 59 (2022) 044003.